The Gas-Phase Photophysics of Eosin Y and its Maleimide Conjugate

S Daly, A Kulesza, G Knight, L Macaleese, Rodolphe Antoine, P Dugourd

The Gas-Phase Photophysics of Eosin Y and its Maleimide Conjugate. S. Daly, A. Kulesza, G. Knight, L. MacAleese, R. Antoine and P. Dugourd. *J. Phys. Chem. A* (2016).
http://dx.doi.org/10.1021/acs.jpca.6b01075

The Gas-Phase Photophysics of Eosin Y and its Maleimide Conjugate.

Steven Daly,[a] Alexander Kulesza,[a] Geoffrey Knight,[a] Luke MacAleese,[a] Rodolphe Antoine[a] and Philippe Dugourd[a].*

a. Institut Lumière Matière, Université Lyon 1 – CNRS, Université de Lyon, 69622 Villeurbanne Cedex, France.

ABSRACT: The use of the xanthene family of dyes as fluorescent probes in a wide range of applications has provided impetus for the studying of their photophysical properties. In particular, recent advances in gas-phase techniques such as FRET that utilize such chromophores have placed a greater importance on the characterization of these properties in the gas-phase. Additionally, the use of synthetic linker chains to graft the chromophores in a site-specific manner to their target system is ubiquitous. There is, however, often limited information on how the addition of such a linker chain may affect the photophysical properties of the chromophores, which is of fundamental importance for interpretation of experimental data reliant on grafted chromophores. Here, we present data on the optical spectroscopy of different protonation states of Eosin Y – a fluorescein derivative. We compare the photophysics of Eosin Y to its maleimide conjugate, and to the thioether product of the reaction of this conjugate with cysteamine. Comparison of the mass spectra following laser irradiation shows that very different relaxation takes place upon addition of the maleimide moiety, but that the photophysics of the bare chromophore are restored upon addition of cysteamine. This radical change in the photophysics is interpreted in terms of charge-transfer states, whose energy relative to the $S_1 \leftarrow S_0$ transition of the chromophore is

dependent on the conjugation of the maleimide moiety. We also show that the shape of the absorption band is unchanged in the gas-phase as compared to the solution-phase, showing a maximum with a shoulder towards the blue, and examination of isotope distributions of the isolated ions show that this shoulder cannot be due to the presence of dimers. Consideration of the fluorescence emission spectrum allows a tentative assignment of the shoulder to be due to a vibrational progression with a high Frank-Condon factor.

Introduction

The xanthene-based dye family – which includes the rhodamines and fluorones – are almost ubiquitous as fluorescent probes with a high quantum yield in a vast range of subject areas, and as such there has been a wealth of studies probing their solution phase properties.[1–5] Eosin Y (EY), one such xanthene derivative, has been studied particularly intensively since it has found a use as a probe for trace amounts of peptide, as a source of singlet molecular oxygen, and as an absorber in dye-sensitized photo-cells.[6–11] The solution phase absorption spectroscopy of Eosin Y has been studied in some detail as a function of the solvent or pH.[12–15] Eosin Y can exist in a number of different protonation states in solutions, ranging from singly protonated $[EY+H]^+$ to double deprotonated $[EY-2H]^{2-}$ due to the presence of both phenolic and carboxylic acid moieties, Figure 1.

Batistela *et al.* found second and third pK_a values of 2.02 and 3.80 to yield $[EY-H]^-$ and $[EY-2H]^{2-}$ respectively.[12] By studying the absorption spectroscopy in H_2O as a function of the pH, they were able to extract values of the absorption maximum of 470 nm, 519 nm and 515 nm for [EY], $[EY-H]^-$ and $[EY-2H]^{2-}$ respectively. The profile of the absorption spectrum for the negatively charged species shows a main peak with a shoulder at higher excitation energies. The origin of this shoulder is most commonly posited to be due to the presence of dimers.[13,16–18] They also found a pronounced change in the absorption band as the pH is increased from 0.31 to 2.95, which they attributed to the coexistence of multiple charge states

in the solution. This coexistence of charge states makes the interpretation of solution phase spectroscopy difficult; particularly since the absorption maxima are close - making their deconvolution difficult.

Alternative to studying pH-dependent absorption in solution, the use of mass spectrometry allows the isolation and subsequent measurement of absorption properties by action-spectroscopy of different charge states independently. The gas-phase spectroscopy of xanthene derivatives has become a common technique in the past decade, and in particular the absorption and fluorescence properties as related to gas-phase Förster Resonance Energy Transfer (FRET).[19–23] Moreover, Eosin Y is potentially attractive as an acceptor chromophore for studies of anion action-FRET since electron detachment has been shown to be an important mechanism in related dyes.[22,23] Additionally, the characterization of any changes in photophysical properties of chromophores following conjugation to a synthetic linker chain – which is used for grafting onto specific sites in proteins or other systems – is vital for interpretation of FRET data. The maleimide moiety is one such linker. It reacts specifically with thiols to form a thioether product, and has been previously shown to influence the photophysics of chromophores, acting as a fluorescence quencher.[24]

In this paper, we aim to unravel the mechanisms leading to the different charge-state dependent photo-processes in conjugated chromophore-maleimide molecules prior to and following the grafting reaction. We address this question by solution-phase absorption measurements of Eosin Y, gas-phase action-spectroscopy measurements on the mono- and dianions of Eosin Y (EY), its maleimide conjugate 5-maleimido-Eosin Y (EYM), and the product of the reaction of EYM with cysteamine (EYM-CA) and excited state computations.

Method

Experimental

2 mg of Eosin Y (EY) (Sigma Aldrich) and 5-maleimido-Eosin Y (EYM) (Sigma Aldrich) were independently dissolved in 200 µL DMSO before subsequent dilution in 5 ml H_2O to a final concentration of 30 µM for use in the electrospray source. 8.2 mg of Cysteamine hydrochloride was dissolved in 1 ml H_2O at a concentration of 7.2 mM. For the reaction of EYM with cysteamine, an equimolar solution of the two reactants was prepared in H_2O at a concentration of 30 µM and left to react at room temperature for 1 hour, after which it was directly used in the electrospray source.

The experimental setup used to perform the experiments presented in this paper has been described in detail previously[19]. Briefly, a linear quadrupole ion trap mass spectrometer (LTQ Velos, Thermo Fisher Scientific, San Jose, CA) was used to generate, mass select, and trap ions in a first, high pressure trap for a controlled period during which time they may be activated by laser irradiation (Laser Induced Dissociation, LID). Fragment ions are subsequently transmitted to a second, lower pressure ion trap, and are mass analyzed. A fused silica window (3 mm thick, 1 in. diameter) is positioned at the back end of the instrument, and 1-2 mm diameter circular openings in the trapping electrodes allow coupling of light source and trapped ions. In order to optimize laser transmission, the central hole of the electrode closest to the fused silica window was enlarged to 5 mm in diameter.

The light source used was a Horizon OPO pumped by the third harmonic of a Surelite II Nd:YAG laser (Continuum, Santa Clara, CA). A repetition rate of 10 Hz and a pulse width of 5 ns were used. The beam was focused into the first ion trap using a 1000 mm focal length convergent lens. A mechanical shutter, synchronized with the mass spectrometer, was used to stop the beam at all times except the “ion activation window”, that is, the time after ion accumulation and before the mass analysis. A single laser pulse was used for the irradiation of the trapped ions, and when irradiating ions the normalized collision energy is kept at zero. To record action spectra, the laser wavelength was scanned between 590 and 420nm, in 0.1 nm

steps and with a 1 s dwell time at each wavelength. During the scan, each data point is the average of 9 mass spectra, which corresponded to on average one data point per second. Laser power was recorded by performing a second scan under identical conditions immediately following acquisition of the action spectrum. To analyze the data, each mass spectrum was assigned a wavelength value given by $\lambda_{start} - \left((i-1) * \left(\frac{\Delta\lambda}{n}\right)\right)$ where $\lambda_{start} = 590$ nm is the starting wavelength, i the mass spectrum number, $\Delta\lambda = 170$ nm is the total wavelength change, and n the total number of mass spectra acquired during the acquisition. The same procedure was used to provide a wavelength range for the laser power (*P*), and a linear interpolation performed to give values of the laser power at the wavelengths assigned to each mass spectrum. The action spectrum is defined as $-\log\left(I_{parent}/I_{total}\right)/(\lambda * P)$ where I_{parent} and I_{total} are the parent and total ion signal respectively at each point in the acquisition.

Solution phase spectroscopy was performed on Eosin Y diluted to 5 μM in H_2O, and the pH was controlled by addition of either ammonium hydroxide or acetic acid. Absorption spectra were performed using an Avantes AvaLight DHS light source and an AvaSpec 2048 spectrometer. The fluorescence excitation spectra were measured on a Fluoromax-4 spectrophotometer (Horiba) by monitoring the fluorescence at 555 nm. The fluorescence emission spectra were measured on the same instrument following excitation at 520 nm.

Theoretical

Gas-phase optimizations and excited state calculations were performed using density functional theory (DFT) and time-dependent DFT (TDDFT) as implemented in Gaussian09 Rev D.01.25 The hybrid CAM-B3LYP[26–28] exchange-correlation functional that provides long-range corrections with the Coulomb attenuation method was used. For all atoms, Ahlrichs triple-ζ plus polarization atomic basis sets were used (def2-TZVP). Optimizations

included Grimme's empirical dispersion correction including Becke-Johnson damping D3(BJ)[29,30.]

Results

Eosin Y (EY) and 5-maleimido-Eosin Y (EYM) – Figure 1 – both contain two possible deprotonation sites; the phenolic acid and carboxylic acid moieties. Previous measurement of EY in solution phase has shown the former as having the lower pK_a value (2.02) compared to the later (3.80).[12] As noted above, given that EY likely exists in multiple charge states in solution, it is difficult to measure the absorption spectrum of individual charge state. However, it is possible in solution to produce predominantly monoanions or dianions of EY by controlling the pH of the solution.[12] As such, the solid blue curves in Figure 2 shows the solution phase spectra of EY in H_2O at pH 2.53 (a) and 11.87 (b), which have been shown to produce predominantly $[EY\text{-}H]^-$ and $[EY\text{-}2H]^{2-}$ respectively. The absorption band shows a similar profile under both conditions, with an absorption maximum at 520 nm for the pH 2.53 solution and 517 nm for the pH 11.87 solution, and a shoulder is observed for both solutions at 492 nm, Table 1. The conventional explanation for the presence of this shoulder in xanthene derivatives is the presence of dimers.[13,16–18] These values are in good agreement with the values of the absorption maximum determined by Batistela *et al*. of 519 and 515 nm respectively for $[EY\text{-}H]^-$ and $[EY\text{-}2H]^{2-}$ respectively.[12]

Upon electrospray ionization of EY and EYM in H_2O, the resulting mass spectrum shows both mono- and dianionic species. Figure 2 shows the gas phase action spectra of mass selected (a) $[EY\text{-}H]^-$ and $[EYM\text{-}H]^-$ and (b) $[EY\text{-}2H]^{2-}$ and $[EYM\text{-}2H]^{2-}$ as black squares and red circles respectively. There is a clear difference in the action spectrum measured for the two species, with $[EY\text{-}H]^-$ showing a broad absorption band with two features at 498 nm and 531 nm, whilst $[EYM\text{-}H]^-$ shows a single peak at 532 nm with a shoulder at 507 mn (Table 1). Similar absorption profiles to that of $[EY\text{-}H]^-$ have been observed in previous action-

spectroscopy studies of fluorescent xanthene dyes, and can be interpreted in terms fluorescence rather than fragmentation being the dominant relaxation mechanism following photoexcitation.[19,31] The fluorescence quantum yield may depend strongly on the excitation energy; low excitation energies leading to ions with minimal vibrational excitation in the excited state is where the fluorescence quantum yield tends to be highest. As the energy is increased, the increased vibrational energy of the excited state can lead to an increased rate of non-fluorescent relaxation pathways – such as direct photofragmentation or an increased rate of internal conversion or intersystem crossing.

The fluorescence quantum yield of EY has been determined to be between 0.15 and 0.22 in water, 0.44 and 0.63 in methanol and 0.4 and 0.72 in ethanol.[32] Additionally, measurements of the gas-phase fluorescence emission spectrum of various halogenated fluorescein derivatives have shown that the monoanions possess a weak but measureable fluorescence quantum yield, and indicated that increased halogenation of fluorescein leads to an increase in the gas-phase fluorescence.[22] We can thus assign the band at 531 nm in the action spectrum of $[EY\text{-}H]^-$ to be the true gas-phase absorption maximum, where the fluorescence quantum yield is high and hence other relaxation channels which may lead to fragmentation are suppressed. Similarly, we assign the band at 498 nm to be the shoulder observed in the solution-phase absorption spectrum. This assignment is supported by the $[EYM\text{-}H]^-$ action spectrum, where the addition of the maleimide moiety is known to cause a fluorescence quenching effect. As such, the shape of the absorption band closely resembles that seen in solution, and the absorption maximum of 532 nm is very close in energy to the first band in $[EY\text{-}H]^-$.

This difference in photophysical behavior with addition of the maleimide moiety is even starker when the dianions are considered. It has been previously observed that dianionic fluorescein and its derivatives are non-fluorescent in the gas phase, and instead relax via photodetachment.[22,23] This is exactly what is observed in $[EY\text{-}2H]^{2-}$ – Figure 3a – and the

action spectrum now resembles very closely the solution-phase spectrum for EY (solid blue curve), with an absorption maximum of 509 nm and a shoulder at 482 nm observed. The absorption band of $[EYM\text{-}2H]^{2-}$ is very similar in appearance to $[EY\text{-}2H]^{2-}$, but with slightly redshifted values of 515 nm and 494 nm for the absorption maximum and shoulder respectively.

This shift already hints that the presence of the maleimide moiety is influencing the first $\pi \rightarrow \pi^*$ transition of the Eosin Y chromophore. Examination of the LID mass spectrum at the absorption maximum shows that relaxation no longer takes place only via photo-detachment but instead by a combination of photo-detachment and photofragmentation (Figure 3b) with fragments at m/z 691, 614 (losses of 45 and 123 Da and corresponding to loss of a charge plus CO_2H and CO_2Br respectively) and 79 (corresponding to Br^-) being the dominant species observed. This difference in behavior indicates that very different excited state dynamics are occurring in the two systems. It is known that the maleimide moiety is able to act as a fluorescence quencher of chromophores, and that upon reaction with a sulfhydryl group to form a thioalkyl succinimide this quenching effect is lost.[24] Guy *et al.* posited that the quenching mechanism is a photo-induced electron transfer from the chromophore to the maleimide, which is consistent with the relaxation mechanism observed here being in direct competition with photo-detachment, a process that occurs on the femtosecond to picosecond timescale.[24]

In order to determine that the observed quenching was quantitatively similar to that observed by Guy *et al*., EYM was reacted with cysteamine to give the thioether EYM-cysteamine product [EYM+CA], Figure 1. The action spectra for the mono- and dianion is shown in Figure 2, and the LID mass spectrum of the dianion at the absorption maximum are shown in panel (c) of Figure 3. The LID mass spectrum shows that photo-detachment is again the dominant relaxation channel of $[EYM+CA\text{-}2H]^{2-}$, closely resembling the case of [EY-

$2H]^{2-}$, rather than $[EYM\text{-}2H]^{2-}$. This indicates that the quenching mechanism of the maleimide group is significantly reduced upon reaction of the maleimide with a thiol – as observed by Guy et al. – although some fragmentation pathways are still observed. Furthermore the absorption maximum of $[EYM+CA\text{-}2H]^{2-}$ is found at 513 nm, which is intermediate to the values for $[EY\text{-}2H]^{2-}$ and $[EYM\text{-}2H]^{2-}$ and hence shows the thioalkyl succinimide perturbs the $S_0 \leftarrow S_1$ transition less than the unreacted maleimide. Equally, the shape of the absorption band of $[EYM+CA\text{-}H]^-$ more closely resembles $[EY\text{-}H]^-$, with a similar suppression of fragmentation yield at low excitation energies being indicative of fluorescence.

What is the origin of the quenching mechanism of the maleimide moiety? As noted above, the large reduction of the branching ratio of photo-detachment may indicative of an electron transfer process in $[EYM\text{-}2H]^{2-}$, which is switched off by the reduction of maleimide to succinimide by the addition of cysteamine to the maleimide. To better understand how this chemical transformation quenches the electron transfer process, calculations on the electron transfer characteristics were performed. The singlet excited states of $[EYM\text{-}2H]^{2-}$ and $[EYM+CA\text{-}2H]^{2-}$ were calculated and the transitions with dominant charge transfer character (CT) identified (long-range corrected hybrid functionals such as CAM-B3LYP have been designed for accurately describing CT types of transitions).

The results of this analysis are given in Figure 4 (see also Table S1 in the SI). CT states can be identified by inspection of the excitations between occupied Kohn-Sham orbitals φ_i and unoccupied ones φ_a. Contrary to the local π-π^* excitation (e.g. S_1 for $[EY\text{-}2H]^{2-}$ in Figure 4), CT excitations involve orbitals localized at different moieties. This locality can be quantified using the spatial overlap O_{ia} defined as the inner product of the moduli of the two orbitals φ_i and φ_a (See SI, Table S1, used also in Tozer's diagnostic test for charge transfer states).[33] A nonlocal CT excitation usually has little spatial overlap ($O_{ia} < 0.1$) as identified also in the leading excitations in the CT states in $[EYM\text{-}2H]^{2-}$ (S_1) and $[EYM+CA\text{-}2H]^{2-}$ (S_4). Both CT

transitions involve excitation from the EY π-system to a π* orbital centered on the maleimide moiety. In the case of EYM this orbital is of pure π* character, whilst for EYM+CA a partial σ* character induced by the reduction of the maleimide to succinimide due to the reaction with cysteamine shifts the entire excited state higher in energy. Thus the CT state is found at 2.3 eV in $[EYM\text{-}2H]^{2-}$ and at about 4.1 eV for the $[EYM+CA\text{-}2H]^{2-}$. The difference in the energy of the CT states is driven by changes in the electron affinity of the maleimide (-0.725 eV) and succinimide (+1.000 eV) moieties.

The position of the CT state in relation to the initially excited EY π-π* governs the final deactivation pathway (the system relaxes from the lowest excited state to the ground state in analogy to Kasha's rule). TDDFT calculations fail to accurately reproduce the transition energy of the first singlet excitations of xanthene derivatives – although it is more successful in the UV.[19,34] The experimentally determined EY π-π* transition energy of 2.44 eV is therefore taken as a reference value for the energetic position of $[EYM\text{-}2H]^{2-}$ and $[EYM+CA\text{-}2H]^{2-}$. Despite of the apparent systematic shift, the trends of TDDFT are still valuable for a comparison across the compounds and included into Figure 4.

This comparison reveals that the π-π* transition energy is unaffected by the functionalization while the energy of the CT state significantly depend on the substitution at the maleimide (see above). In particular, the CT state in $[EYM\text{-}2H]^{2-}$ is found below the π-π* transition by ~ 0.1 eV. This renders the conversion to the CT state possible for $[EYM\text{-}2H]^{2-}$ but not for $[EYM+CA\text{-}2H]^{2-}$ suggesting an electron-transfer enabled deactivation pathway for $[EYM\text{-}2H]^{2-}$.

It is thus possible to posit an explanation for differences in photophysical behavior of EY attached to either maleimide or succinimide moieties. In $[EYM+CA\text{-}2H]^{2-}$ the excitation is localized on the xanthene moiety and photo-detachment is likely to occur from here, producing a single radical center. In $[EYM\text{-}2H]^{2-}$, the fast internal conversion to the CT state

followed by photo-detachment will lead to the radical center being in a different location, which may give a more reactive monoanion radical species and hence lead to enhanced unimolecular fragmentation of the resulting system.

Finally, it is interesting to consider the origin of the shoulder which is observed in both solution- and gas-phase spectra. This shoulder is commonly attributed to the presence of dimers in solution-phase absorption spectroscopy, but in the gas-phase it is possible to unambiguously check for the presence of dimers. As the mass-to-charge ratio of, for example, $[EYM\text{-}nH]^{n-}$ and $[EYM\text{-}nH]_2^{2n-}$ will be the same, in order to discount the possibility of there being any dimers present during our isolation step it is important to examine the isotopic distribution we obtain when isolating both $[EYM\text{-}H]^-$ and $[EYM\text{-}2H]^{2-}$. Figure 5 shows the experimental and simulated isotopic distributions for $[EYM\text{-}H]^-$ (a and b) and $[EYM\text{-}2H]^{2-}$ (c and d), where the broadening of the distribution is due to the isotopes of bromine.

There is no evidence for the presence of dimers during the isolation of either species, and thus the origin of the shoulder in the gas-phase action spectra cannot be attributed to the presence of dimers. This is consistent with previous gas phase measurements of rhodamine derivatives, where similar profiles to those observed in solution are also found, and indeed with other poly-aromatic dyes, indicating this may be a more general phenomenon.[20,22,23,35,36] Additionally, gas-phase action spectroscopy performed upon pseudo-dimers of rhodamine 575, where the dimerization is created by enforced proximity of the dyes following grafting onto a tri-peptide, shows there is only a small shift in the position of the absorption maximum relative to the monomeric species.[31] Moreover, recent solution phase measurements of pyronin B dimers in solution found their absorption and fluorescence properties to differ only very slightly from the monomer.[37]

Where then does the origin of this shoulder then lie? The possibility of their being a second singlet excitation close to the $S_1 \leftarrow S_0$ transition, or that there be a second tautomer (for

example the lactone tautomer which is found in solution for xanthene dyes with underivatized carboxylic acid moieties) can be discounted by examination of the fluorescence spectrum. Following excitation at the absorption maximum of EY at pH 2.43 and 11.87, the fluorescence emission spectrum possesses a red shoulder in both cases (Figures S1 and S2 respectively). Similar behavior is found in a range of different xanthene-based chromophores, in both solution- and gas-phases, strongly indicating that the shoulder is an intrinsic property of the $S_1 \leftarrow S_0$ transition.[15,20,38–40] The fact that the mirror-image rule is obeyed by xanthene derivatives and that the Stoke's shift is small (21 nm for both mono- and di-anions of Eosin Y measured here) indicates that the ground and excited states geometries are similar, and that the shoulder may be ascribed to vibronic transitions in either absorption or emission spectra with strong Franck-Condon factors, see Figure S3.

There are previous solution- and gas-phase measurements of the ground state vibrations of fluorescein and some of its halogenated derivatives such as EY in solution by FTIR and Raman spectroscopy, and in the gas-phase by IRMPD.[41–43] Narayaman *et al.* found that the FTIR of EY in solution contains many intense absorption features between 1000 and 2000 cm^{-1}. Yao *et al*. measured gas-phase fluorescein and 2',7'-dichlorofluorescein by IRMPD action spectroscopy and found a similar series of intense vibrational transitions in the same energy range. They also performed vibrational calculations to assign the observed bands to normal modes, and found that the most intense bands can be assigned to xanthene-based vibrational modes.[43] That the shoulder may be due to a vibrational progression based on the xanthene ring system is supported by the fact that the S_1 absorption profile of xanthene derivatives generally exhibit similar profiles, which would indicate that the origin of the shoulder lies in a common element of this dye family. Particularly, the presence of a shoulder in the solution phase absorption spectrum of acridine red – which contains only the xanthene moiety with no carboxyphenyl moiety – provides support for this assignment.[37] Hence, it

seems that the shape of the S_1 absorption band of xanthene derivatives can be tentatively assigned as being due to the vibrational profile of the $S_1 \leftarrow S_0$ transition.

Conclusions

The gas phase action-spectra of the mono- and dianionic forms of Eosin Y and 5-maleimido-Eosin Y, and the thioether product of the reaction of the latter with cysteamine have been presented. A difference in the action-spectra of the anions of EY and EYM can be interpreted in terms of fluorescence of the former being an important relaxation channel, whilst the maleimide group of the latter acts as a fluorescence quencher. The presence of both photo-fragmentation and photo-detachment in the dianion of EYM supports the idea of photo-induced electron transfer posited by Guy et al. Excited state calculations further suggest a low-lying charge-transfer singlet state in EYM, whose population transfers electron density from the EY to the maleimide π systems and enables alternative deactivation channels to be accessed. This situation is only present with the maleimide providing an exo-energetic electron attachment energy, while reaction with cysteamine no longer allows this “pull”-effect to take place, and thus quenches this electron-transfer. This correlates with the observation that upon grafting of cysteamine to EYM, the photophysical properties of the resultant species are very similar to those of the bare chromophore. These observations are of high importance in all situations where such linker chains are used for specific grafting of chromophores, where the photophysics of the chromophore is of paramount importance for interpretation of data.

The solution-phase absorption spectrum and gas-phase action spectrum both show an absorption maximum with a shoulder to higher energy. The isotope distribution for mass-selected anion and dianion EY derivatives in the gas-phase showed no evidence of dimers, to which this shoulder is commonly attributed, which in turn indicates that the presence of dimers is equally unlikely to be the origin of the shoulder in the solution-phase. Analysis of

the fluorescence emission spectrum following excitation at the absorption maximum in solution indicated that the shoulder is an intrinsic property of the S1 ← S0 transition, and thus could be tentatively assigned to be due to a vibrational progression with a high Franck-Condon factor, with xanthene based vibrational normal modes potentially implicated. This enhanced understanding may be of importance in solution phase where xanthene derivatives are ubiquitous in their use as fluorescent reporters.

ASSOCIATED CONTENT

Details of the TDDFT calculations, and solution phase fluorescence excitation and emission spectra for Eosin Y at pH 2.53 and pH 11.87 may be found in the supplementary information. This material is available free of charge via the Internet at http://pubs.acs.org.

AUTHOR INFORMATION

Corresponding Author

* To whom correspondence should be addressed. Email: philippe.dugourd@univ-lyon1.fr. Telephone: +33 4 72 44 83 21

Author Contributions

All authors have given approval to the final version of the manuscript.

ACKNOWLEDGMENT

The research leading to these results has received funding from the European Research Council under the European Union's Seventh Framework Programme (FP7/2007-2013 Grant agreement N°320659). We gratefully acknowledge computer time granted by the PSMN (Pôle Scientifique de Modélisation Numérique) computing center of ENS de Lyon. A.K. acknowledges support by COST Action CM1405.

References

(1) Arbeloa, F. L.; Arbeloa, T. L.; Estevez, M. J. T.; Arbeloa, I. L. Photophysics of Rhodamines - Molecular-Structure and Solvent Effects. *J. Phys. Chem.* **1991**, *95*, 2203–2208.

(2) Arbeloa, T. L.; Estevez, M. J. T.; Arbeloa, F. L.; Aguirresacona, I. U.; Arbeloa, I. L. Luminescence Properties of Rhodamines in Water-Ethanol Mixtures. *J. Lumin.* **1991**, *48-9*, 400–404.

(3) Arden, J.; Deltau, G.; Huth, V.; Kringel, U.; Peros, D.; Drexhage, K. H. Fluorescence and Lasing Properties of Rhodamine Dyes. *J. Lumin.* **1991**, *48-9*, 352–358.

(4) Magde, D.; Rojas, G. E.; Seybold, P. G. Solvent Dependence of the Fluorescence Lifetimes of Xanthene Dyes. *Photochem. Photobiol.* **1999**, *70*, 737–744.

(5) Karstens, T.; Kobs, K. Rhodamine-B and Rhodamine-101 as Reference Substances for Fluorescence Quantum Yield Measurements. *J. Phys. Chem.* **1980**, *84*, 1871–1872.

(6) Waheed, A. A.; Gupta, P. D. Estimation of Submicrogram Quantities of Protein Using the Dye Eosin Y. *J. Biochem. Biophys. Methods* **2000**, *42*, 125–132.

(7) Waheed, A. A.; Rao, K. S.; Gupta, P. D. Mechanism of Dye Binding in the Protein Assay Using Eosin Dyes. *Anal. Biochem.* **2000**, *287*, 73–79.

(8) Amatguerri, F.; Lopezgonzalez, M. M. C.; Martinezutrilla, R.; Sastre, R. Singlet Oxygen Photogeneration by Ionized and Un-Ionized Derivatives of Rose-Bengal and Eosin Y in Diluted Solutions. *J. Photochem. Photobiol. a-Chemistry* **1990**, *53*, 199–210.

(9) Tai, W. P.; Inoue, K. Eosin Y-Sensitized Nanostructured SnO2/TiO2 Solar Cells. *Mater. Lett.* **2003**, *57*, 1508–1513.

(10) Kim, S. S.; Yum, J. H.; Sung, Y. E. Improved Performance of a Dye-Sensitized Solar Cell Using a TiO2/ZnO/Eosin Y Electrode. *Sol. Energy Mater. Sol. Cells* **2003**, *79*, 495–505.

(11) Jin, Z. L.; Zhang, X. J.; Li, Y. X.; Li, S. B.; Lu, G. X. 5.1% Apparent Quantum Efficiency for Stable Hydrogen Generation over Eosin-Sensitized CuO/TiO2 Photocatalyst under Visible Light Irradiation. *Catal. Commun.* **2007**, *8*, 1267–1273.

(12) Batistela, V. R.; Pellosi, D. S.; de Souza, F. D.; da Costa, W. F.; de Oliveira Santin, S. M.; de Souza, V. R.; Caetano, W.; de Oliveira, H. P. M.; Scarminio, I. S.; Hioka, N. pKa Determinations of Xanthene Derivates in Aqueous Solutions by Multivariate Analysis Applied to UV–Vis Spectrophotometric Data. *Spectrochim. Acta Part A Mol. Biomol. Spectrosc.* **2011**, *79*, 889–897.

(13) Chakraborty, M.; Panda, A. K. Spectral Behaviour of Eosin Y in Different Solvents and Aqueous Surfactant Media. *Spectrochim. Acta Part A Mol. Biomol. Spectrosc.* **2011**, *81*, 458–465.

(14) Zhang, X.-F.; Zhang, Y.; Liu, L. Fluorescence Lifetimes and Quantum Yields of Ten Rhodamine Derivatives: Structural Effect on Emission Mechanism in Different Solvents. *J. Lumin.* **2014**, *145*, 448–453.

(15) Zhang, X.-F.; Zhang, J.; Liu, L. Fluorescence Properties of Twenty Fluorescein Derivatives: Lifetime, Quantum Yield, Absorption and Emission Spectra. *J. Fluoresc.* **2014**, *24*, 819–826.

(16) Chambers, R. W.; Kajiwara, T.; Kearns, D. R. Effect of Dimer Formation on Electronic Absorption and Emission-Spectra of Ionic Dyes - Rhodamines And Other Common Dyes. *J. Phys. Chem.* **1974**, *78*, 380–387.

(17) De, S.; Das, S.; Girigoswami, A. Environmental Effects on the Aggregation of Some Xanthene Dyes Used in Lasers. *Spectrochim. Acta Part a-Molecular Biomol. Spectrosc.* **2005**, *61*, 1821–1833.

(18) Suradkar, Y. R.; Bhagwat, S. S. CMC Determination of an Odd Carbon Chain Surfactant (C13E20) Mixed with Other Surfactants Using a Spectrophotometric Technique. *J. Chem. Eng. Data* **2006**, *51*, 2026–2031.

(19) Daly, S.; Kulesza, A.; Knight, G.; MacAleese, L.; Antoine, R.; Dugourd, P. Visible and Ultraviolet Spectroscopy of Gas Phase Rhodamine 575 Cations. *J. Phys. Chem. A* **2015**, *119* , 5634–5641.

(20) Sagoo, S. K.; Jockusch, R. A. The Fluorescence Properties of Cationic Rhodamine B in the Gas Phase. *J. Photochem. Photobiol. A Chem.* **2011**, *220*, 173–178.

(21) Bian, Q.; Forbes, M. W.; Talbot, F. O.; Jockusch, R. A. Gas-Phase Fluorescence Excitation and Emission Spectroscopy of Mass-Selected Trapped Molecular Ions. *Phys. Chem. Chem. Phys.* **2010**, *12*, 2590.

(22) Yao, H.; Jockusch, R. A. Fluorescence and Electronic Action Spectroscopy of Mass-Selected Gas-Phase Fluorescein, 2',7'-Dichlorofluorescein, and 2',7'-Difluorofluorescein Ions. *J. Phys. Chem. A* **2013**, *117*, 1351–1359.

(23) McQueen, P. D.; Sagoo, S.; Yao, H.; Jockusch, R. A. On the Intrinsic Photophysics of Fluorescein. *Angew. Chemie Int. Ed.* **2010**, *49*, 9193–9196.

(24) Guy, J.; Caron, K.; Dufresne, S.; Michnick, S. W.; Skene; Keillor, J. W. Convergent Preparation and Photophysical Characterization of Dimaleimide Dansyl Fluorogens: Elucidation of the Maleimide Fluorescence Quenching Mechanism. *J. Am. Chem. Soc.* **2007**, *129*, 11969–11977.

(25) Frisch, M. J.; Trucks, G. W.; Schlegel, H. B.; Scuseria, G. E.; Robb, M. A.; Cheeseman, J. R.; Scalmani, G.; Barone, V.; Mennucci, B.; Petersson, G. A.; et al. Gaussian 09, Revision D.01. Gaussian, Inc., Wallingford CT, 2009.

(26) Becke, A. Density Functional Thermochemistry III The Role of Exact Exchange. *J. Chem. Phys.* **1993**, *98*, 5648–5652.

(27) Perdew, J.; Burke, K.; Ernzerhof, M. Generalized Gradient Approximation Made Simple. *Phys. Rev. Lett.* **1996**, *77*, 3865–3868.

(28) Yanai, T.; Tew, D. P.; Handy, N. C. A New Hybrid Exchange-Correlation Functional Using the Coulomb-Attenuating Method (CAM-B3LYP). *Chem. Phys. Lett.* **2004**, *393*, 51–57.

(29) Grimme, S.; Ehrlich, S.; Goerigk, L. Effect of the Damping Function in Dispersion Corrected Density Functional Theory. *J. Comput. Chem.* **2011**, *32*, 1456–1465.

(30) Grimme, S.; Antony, J.; Ehrlich, S.; Krieg, H. A Consistent and Accurate Ab Initio Parametrization of Density Functional Dispersion Correction (DFT-D) for the 94 Elements H-Pu. *J. Chem. Phys.* **2010**, *132*, 154104.

(31) Daly, S.; Poussigue, F.; Simon, A.-L.; MacAleese, L.; Bertorelle, F.; Chirot, F.; Antoine, R.; Dugourd, P. Action-FRET: Probing the Molecular Conformation of Mass-Selected Gas-Phase Peptides with Förster Resonance Energy Transfer Detected by Acceptor-Specific Fragmentation. *Anal. Chem.* **2014**, *86*, 8798–8804.

(32) Penzkofer, A.; Beidoun, A.; Daiber, M. Intersystem-Crossing and Excited-State Absorption in Eosin Y Solutions Determined by Picosecond Double Pulse Transient Absorption Measurements. *J. Lumin.* **1992**, *51*, 297–314.

(33) Peach, M. J. G.; Benfield, P.; Helgaker, T.; Tozer, D. J. Excitation Energies in Density Functional Theory: An Evaluation and a Diagnostic Test. *J. Chem. Phys.* **2008**, *128*, 044118.

(34) Savarese, M.; Aliberti, A.; De Santo, I.; Battista, E.; Causa, F.; Netti, P. A.; Rega, N. Fluorescence Lifetimes and Quantum Yields of Rhodamine Derivatives: New Insights from Theory and

Experiment. *J. Phys. Chem. A* **2012**, *116*, 7491–7497.

(35) Loison, C.; Antoine, R.; Broyer, M.; Dugourd, P.; Guthmuller, J.; Simon, D. Microsolvation Effects on the Optical Properties of Crystal Violet. *Chem. - A Eur. J.* **2008**, *14*, 7351–7357.

(36) Drink, E.; Dugourd, P.; Dumont, E.; Aronssohn, N.; Antoine, R.; Loison, C. Optical Properties of Prodigiosin and Obatoclax: Action Spectroscopy and Theoretical Calculations. *Phys. Chem. Chem. Phys.* **2015**, *17*, 25946–25955.

(37) Zhang, X.-F.; Zhang, J.; Lu, X. The Fluorescence Properties of Three Rhodamine Dye Analogues: Acridine Red, Pyronin Y and Pyronin B. *J. Fluoresc.* **2015**, *25*, 1151–1158.

(38) Forbes, M. W.; Jockusch, R. A. Gas-Phase Fluorescence Excitation and Emission Spectroscopy of Three Xanthene Dyes (Rhodamine 575, Rhodamine 590 and Rhodamine 6G) in a Quadrupole Ion Trap Mass Spectrometer. *J. Am. Soc. Mass Spectrom.* **2011**, *22*, 93–109.

(39) Klonis, N.; Sawyer, W. H. . Spectral Properties of the Prototropic Forms of Fluorescein in Aqueous Solution. *J. Fluoresc.* **1996**, *6*, 147–157.

(40) Sjoback, R.; Nygren, J.; Kubista, M. Absorption and Fluorescence Properties of Fluorescein. *Spectrochim. Acta Part a-Molecular Biomol. Spectrosc.* **1995**, *51*, L7–L21.

(41) Narayanan, V. A.; Stokes, D. L.; Vo-Dinh, T. Vibrational Sprectral Analysis of Eosin Y and Erytheosin B - Intensity Studies for Quantiative Detection by Dyes. *J. Raman Spectrosc.* **1994**, *24*, 415–422.

(42) Wang, L.; Roitberg, A.; Meuse, C.; Gaigalas, A. K. Raman and FTIR Spectroscopies of Fluorescein in Solution. *Spectrochim. Acta Part A Mol. Biomol. Spectrosc.* **2001**, *57*, 1781–1791.

(43) Yao, H.; Steill, J. D.; Oomens, J.; Jockusch, R. A. Infrared Multiple Photon Dissociation Action-Spectroscopy and Computational Studies of Mass-Selected Gas-Phase Fluorescein and 2',7'-Dichlorofluorescein Ions. *J. Phys. Chem. A* **2011**, *115*, 9739–9747.

[EY]

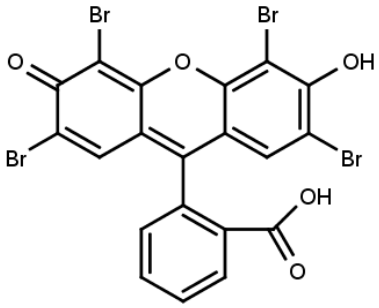

[EYM]

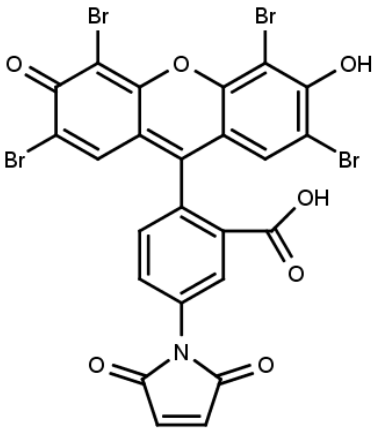

[EYM+CA]

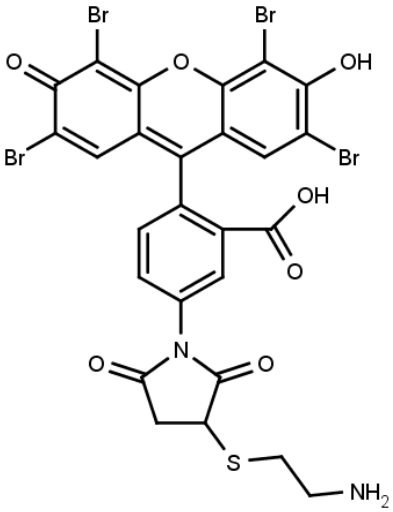

Figures and Tables.

Figure 1. The structure of Eosin Y (EY), 5-maleimido-Eosin Y (EYM), and the product of the addition of cysteamine to 5-maleimido-Eosin Y (EYM+CA).

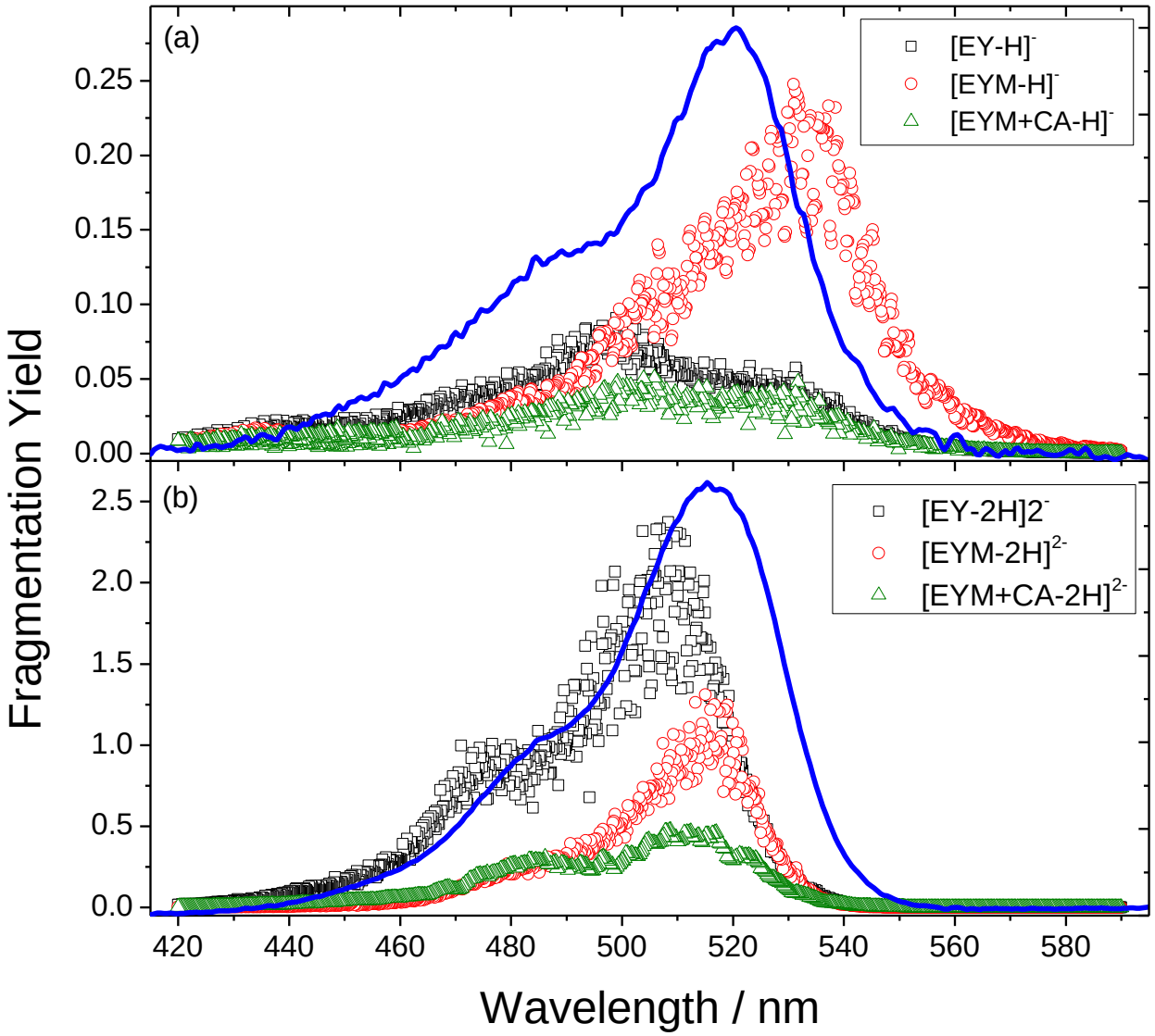

Figure 2. Gas phase action spectra of monoanions (a) and dianions (b) of EY (black squares), EYM (red circles) and EYM+CA, alongside solution phase absorption spectra of EY (solid blue curve) in H_2O at pH 2.53 (a) and 11.87 (b)

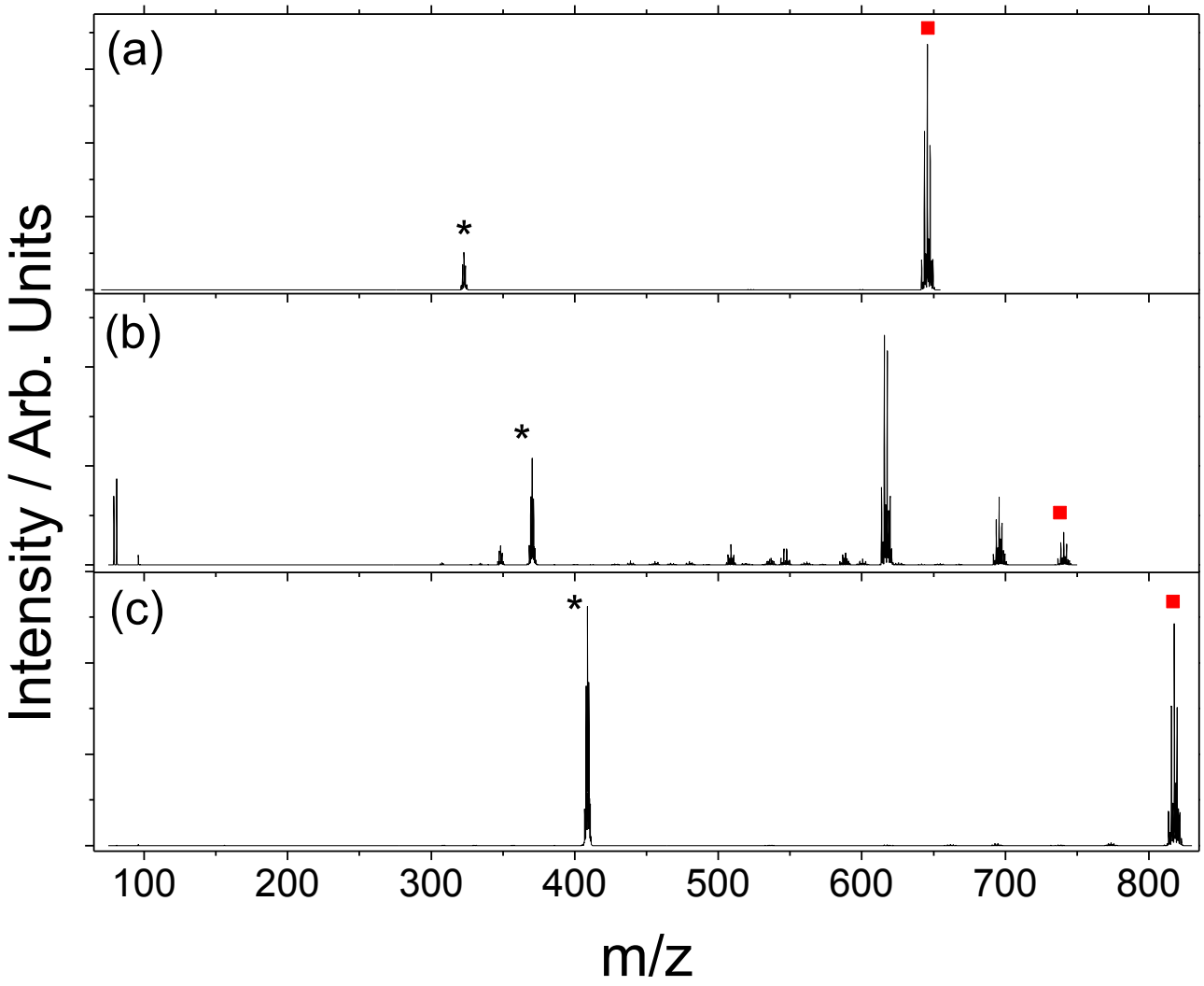

Figure 3. LID mass spectrum of mass selected $[EY\text{-}2H]^{2-}$ (a), $[EYM\text{-}2H]^{2-}$ (b) and $[EYM+CA\text{-}2H]^{2-}$ (c). In each case the asterisk denotes the parent ion, and the red square the photo-detachment channel. All other peaks correspond to fragmentation of the parent ion. The broadening of the peaks is caused by the isotope distribution of Bromine.

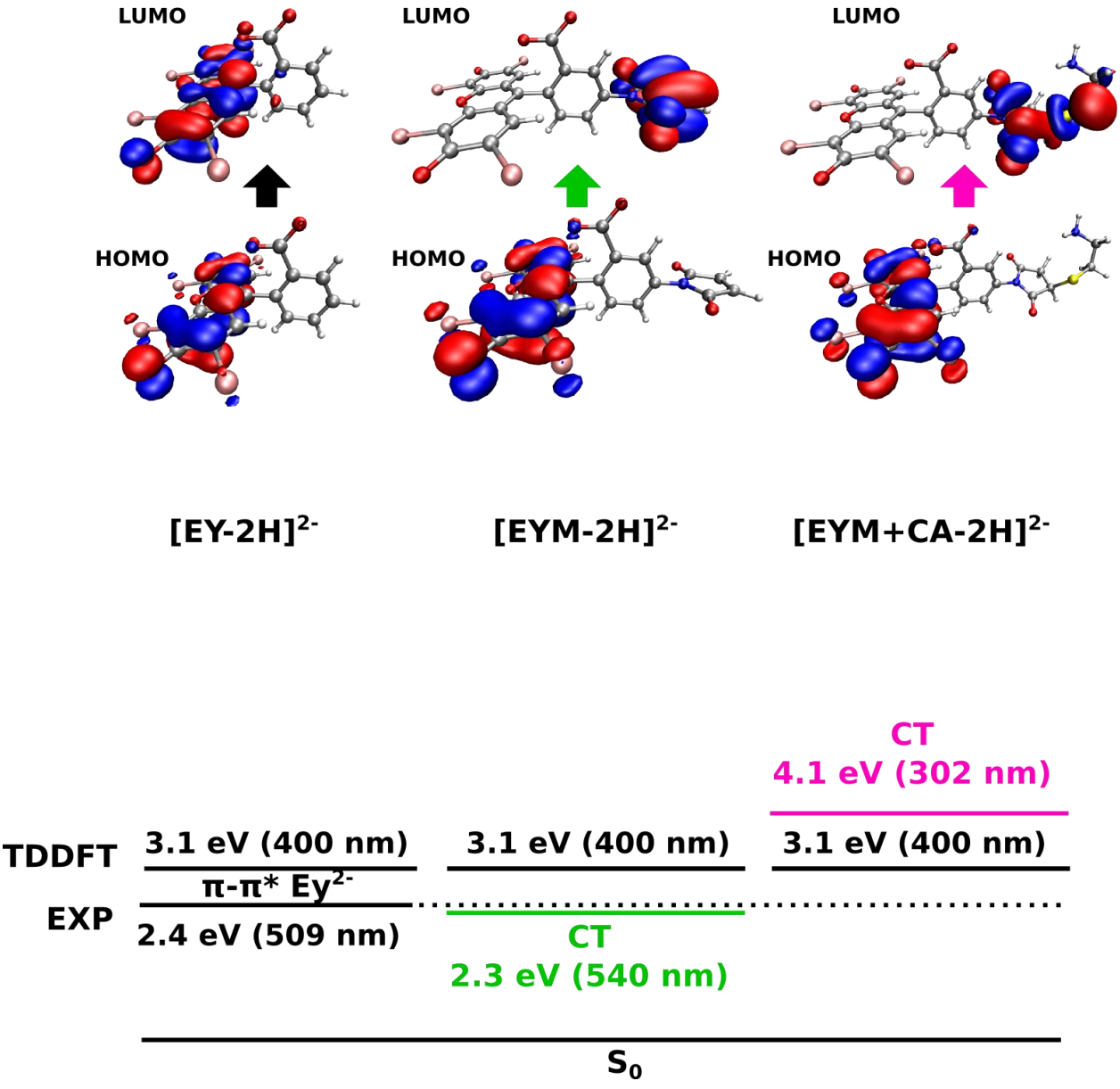

Figure 4. Analysis of the theoretically obtained excited charge-transfer (CT) states of $[EYM\text{-}2H]^{2-}$ (green) and $[EYM+CA\text{-}2H]^{2-}$ (purple). CT states were identified by a dominant excitation between an occupied Eosin Y centered orbital (HOMO) and an unoccupied maleimide centered orbital (LUMO), exhibiting a negligible special overlap, see main text and details of TDDFT excited states given in SI. The TDDFT π-π* energies (black, involved orbitals added for $[EY\text{-}2H]^{2-}$). The experimentally

obtained $[EY\text{-}2H]^{2-}$ π-π* transition energy (EXP) is added as (dashed) black line to indicate the expected π-π* transition energy for all compounds.

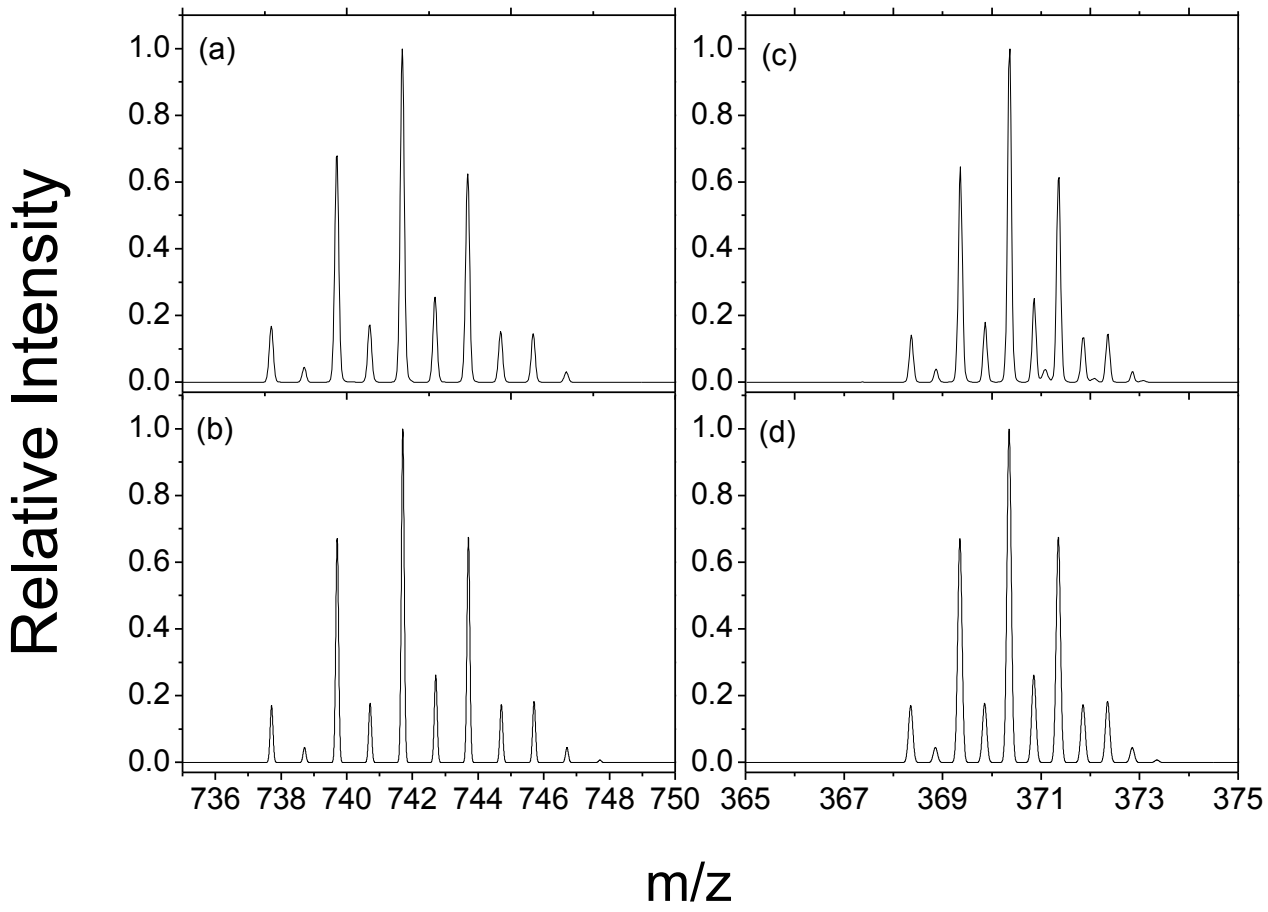

Figure 5. Experimental and theoretical isotopic distribution for mass-selected $[EYM-H]^-$ (a) and (b) respectively and $[EYM-2H]^{2-}$(c) and (d) respectively

Table1. Values for the absorption maximum and shoulder of anionic Eosin Y derivatives in solution and gas phase.

Species	Solution-phase absorption maximum / nm (shoulder in parentheses)	Gas-phase absorption maximum / nm (shoulder in parentheses)
$[EY\text{-}H]^-$	520 (492)[a]	531 (498)
$[EY\text{-}2H]^{2-}$	517 (492)[b]	509 (482)
$[EYM\text{-}H]^-$	-	532 (507)
$[EYM\text{-}2H]^{2-}$	-	516 (496)
$[EYM+CA\text{-}H]^-$	-	531 (503)
$[EYM+CA\text{-}2H]^{2-}$	-	513 (484)

[a] taken in H_2O pH 2.53, [b] taken in H_2O pH 10.87.

TOC graphic

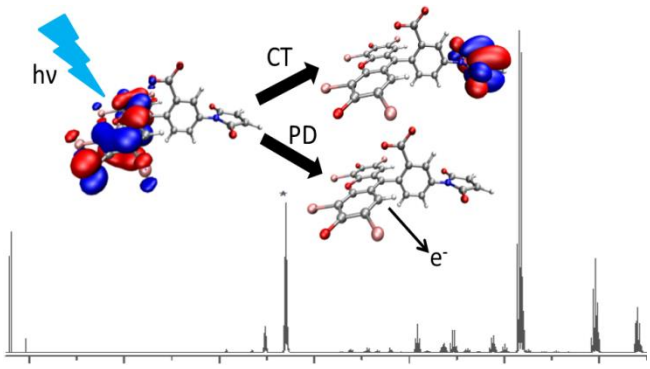

Competition between charge transfer or photodetachment occurs following photoexcitation of Eosin Y maleimide depending upon the conjugation of the maleimide.

The Gas-Phase Photophysics of Eosin Y and its Maleimide Conjugate.

Steve Daly,[a] Alexander Kulesza,[a] Geoffrey Knight,[a] Luke MacAleese,[a] Rodolphe Antoine[a] and Philippe Dugourd[a].*

a. Institut Lumière Matière, Université Lyon 1 – CNRS, Université de Lyon, 69622 Villeurbanne Cedex, France.

Table S1. Details of the relevant TDDFT results (c.f. Figure 4).

Excited State	KS-Orbital Excitation	TDDFT Coefficient X_{ia}	Spacial Overlap $O_{ia} = \langle \lvert\varphi_i\rvert \lvert\varphi_a\rvert \rangle$
$[EY-2H]^{2-}$			
S_1 (3.1 eV, f=0.8)	HOMO → LUMO	0.7	0.64 (π- π*)
$[EYM-2H]^{2-}$			
S_1 (2.3 eV, f=0.0)	HOMO → LUMO	0.7	0.004 (CT)
S_3 (3.1 eV, f=0.3)	HOMO-3 → LUMO HOMO → LUMO+1	0.49 0.42	0.025 (CT) 0.64 (π- π*)
$[EYM+CA-2H]^{2-}$			

S_1 (3.1 eV, f=0.8)	HOMO → LUMO+1	0.7	0.65 (π- π*)
S_4 (4.07 eV, f=0.0)	HOMO → LUMO	0.7	0.066 (CT)

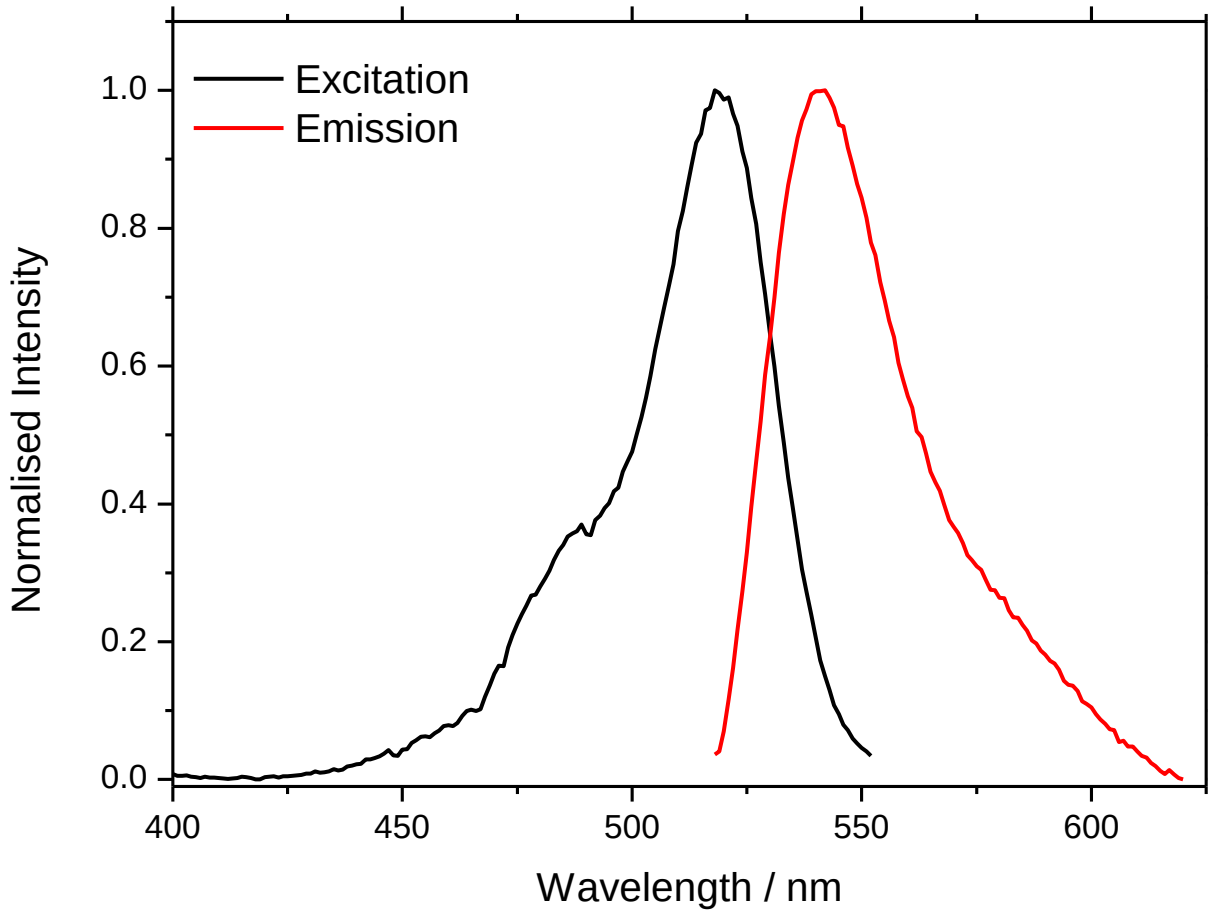

Figure S1. Fluorescence excitation (black) and emission (red) spectra of Eosin Y in H_2O at pH 2.53.

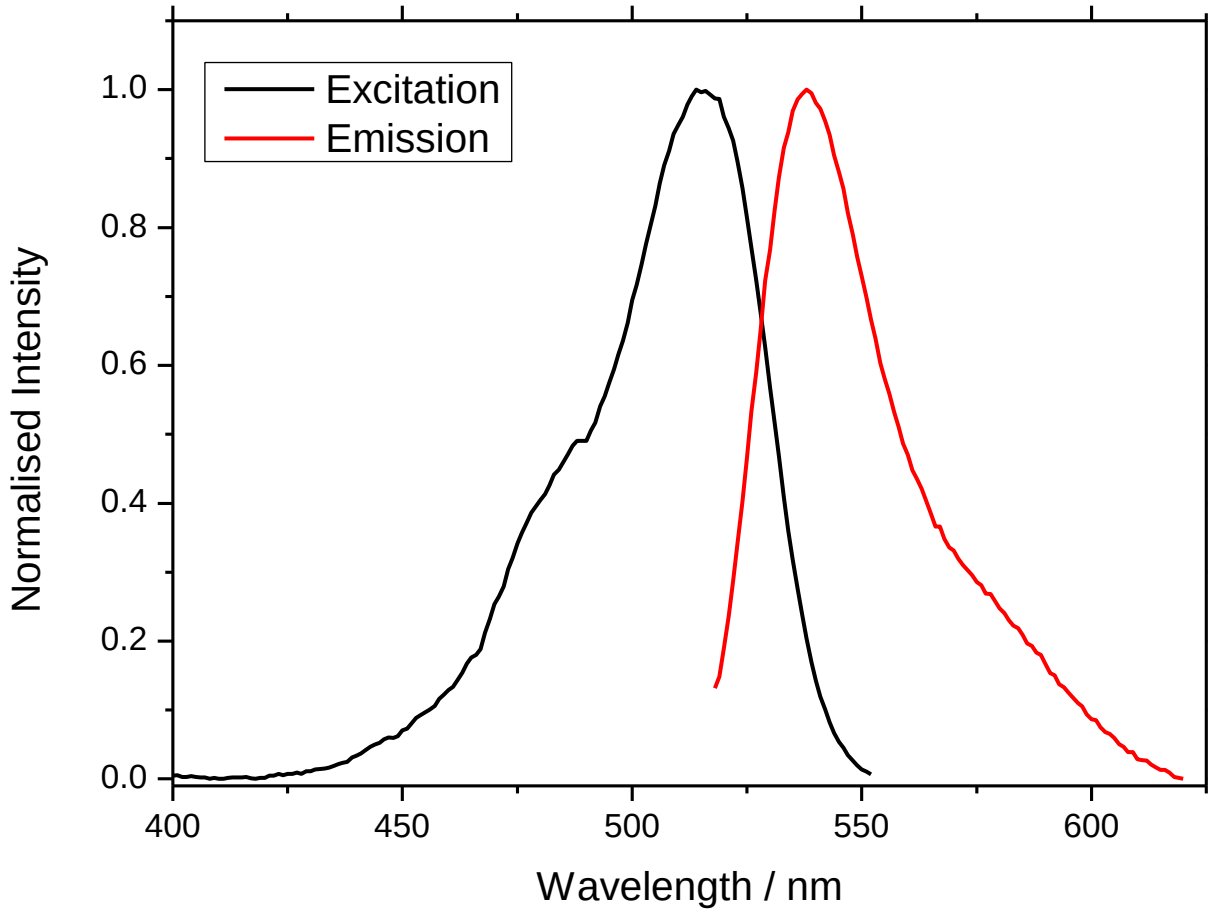

Figure S2. Fluorescence excitation (black) and emission (red) spectra of Eosin Y in H_2O at pH 11.87.

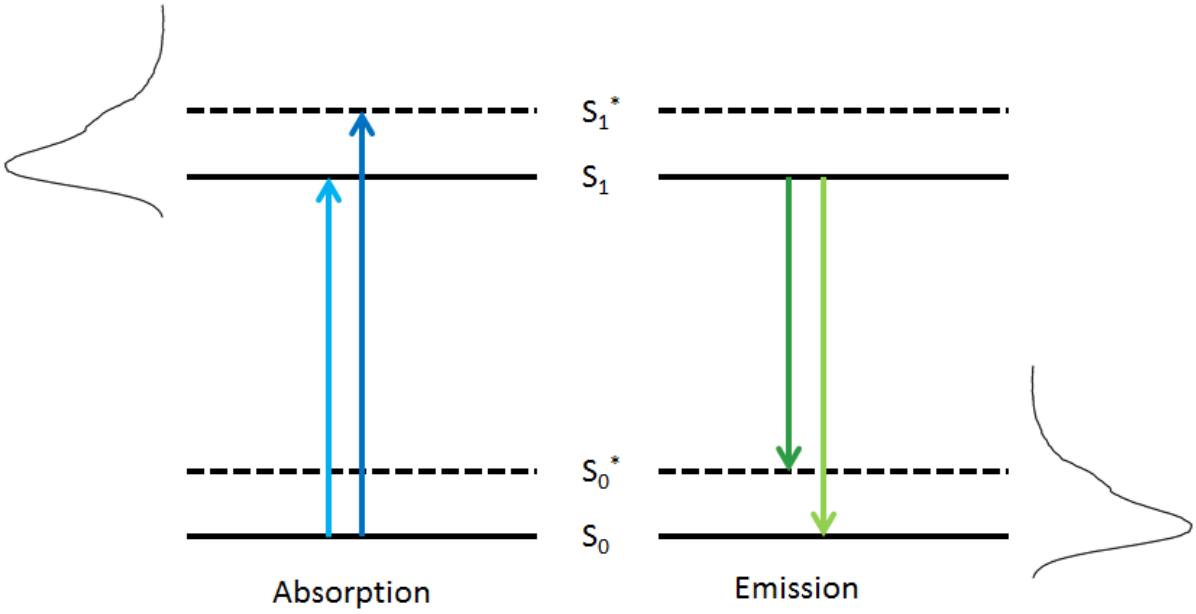

Figure S3. Schematic diagram of the absorption and emission processes leading to the observation of a shoulder in both the absorption and fluorescence spectrum of Eosin Y. Here, S_0 and S_1 refer to the ground and first excited state of the system, and S_0* and S_1* refer to a vibrational level within the ground and first excited state respectively.

Table S2. Fitted values for the fluorescence excitation and emission spectra of Eosin Y in H_2O at different values of the pH.

pH	Excitation (shoulder) / nm	Emission (shoulder) / nm
2.53	520 (492)	541 (567)
11.87	517 (492)	538 (362)